nature cell biology

An actomyosin-based barrier inhibits cell mixing at compartmental boundaries in *Drosophila* embryos

Bruno Monier[1,3,4], Anne Pélissier-Monier[1,2,3], Andrea H. Brand[1,2] and Bénédicte Sanson[1,4]

Partitioning tissues into compartments that do not intermix is essential for the correct morphogenesis of animal embryos and organs[1–3]. Several hypotheses have been proposed to explain compartmental cell sorting, mainly differential adhesion[1–9], but also regulation of the cytoskeleton[10,11] or of cell proliferation[10,12]. Nevertheless, the molecular and cellular mechanisms that keep cells apart at boundaries remain unclear. Here we demonstrate, in early *Drosophila melanogaster* embryos, that actomyosin-based barriers stop cells from invading neighbouring compartments. Our analysis shows that cells can transiently invade neighbouring compartments, especially when they divide, but are then pushed back into their compartment of origin. Actomyosin cytoskeletal components are enriched at compartmental boundaries, forming cable-like structures when the epidermis is mitotically active. When MyoII (non-muscle myosin II) function is inhibited, including locally at the cable by chromophore-assisted laser inactivation (CALI)[13,14], in live embryos, dividing cells are no longer pushed back, leading to compartmental cell mixing. We propose that local regulation of actomyosin contractibility, rather than differential adhesion, is the primary mechanism sorting cells at compartmental boundaries.

During animal development, discrete developmental units called compartments are separated by boundaries of lineage restriction, which stop cells with different identities from mixing. In addition, compartmental boundaries often localize signalling centres. Segregating cell populations at compartmental boundaries is therefore essential for the correct patterning and differentiation of surrounding tissues[1–3]. This organizing principle is conserved from flies to humans. In humans, cell sorting defects during compartmentalization are thought to cause malignant invasion and congenital defects such as craniofrontonasal syndrome[15–17]. In the vertebrate hindbrain rhombomeres and in the *Drosophila* wing disc, cell sorting between compartments is governed both by transcription factors that confer compartment-specific identities and by signalling localized to the boundaries, such as EPH–Ephrin, Hedgehog or Notch signalling[4,18–26]. Downstream of these factors, several mechanisms have been proposed for cell sorting, mainly differential adhesion[1–9], but also regulation of the cytoskeleton[10,11], regulation of cell proliferation[10,12] or extracellular matrix fences[3]. However, *in vivo* support for these hypotheses is scarce and the molecular and cellular mechanisms sorting cells at compartmental boundaries remain unclear.

Here, we investigate this problem in the early *Drosophila* embryo. During segmentation, the trunk is divided into alternating anterior and posterior compartments (Fig. 1a)[27]. Anterior cells, which express the Wnt-1 homologue Wingless (Wg), and posterior cells, which express the homeodomain protein Engrailed (En), are separated by parasegmental boundaries, which behave as boundaries of lineage restriction (they stop cell mixing) during stages 8–11 of embryogenesis (ref. 28). The posterior interface at the En stripe (where the segment border will form at a later stage) is not a barrier to cell mixing at these stages[28].

We found that during stages 8–11, cells on both sides of the PS boundary minimize their contacts, forming a straight line of adjoining membrane interfaces (Fig. 1b). When compartmentalization was compromised, as in *wg* mutants, membrane alignment was lost and some cells invaded the opposite compartment (Fig. 1c). We quantified the degree of misalignment by measuring an index of straightness (IS) for a row of interfaces: the straighter the row, the closer the IS to 0, which corresponds to a straight line. Quantification confirmed that PS boundary interfaces were significantly straighter than other dorso-ventral columns of interfaces (Fig. 1d; IS = 3.7 ± 0.4 for PS boundaries and IS = 14.2 ± 1.1 for other interfaces, $n = 25$). In wg^{CX4} mutant embryos, the interfaces that should have formed PS boundaries had an IS of 14.8 ± 1.0 ($n = 24$), which was similar to the IS of non-boundary interfaces in wild-type embryos (Fig. 1d). We conclude that membrane alignment is a property of lineage restriction boundaries in the *Drosophila* embryo.

To identify effector genes required for cell sorting at PS boundaries, we screened for genomic deletions that give rise to an altered *en* expression pattern. We recovered several deletions that caused embryos to have irregular boundaries reminiscent of loss-of-compartmentalization phenotypes (Supplementary Information, Fig. S1). Several of these deletions removed at least one regulator of the Wg signalling pathway, consistent with its role in anterior/posterior compartmentalization. One small deletion, however,

[1]Department of Physiology, Development and Neuroscience, University of Cambridge, Downing Street, Cambridge CB2 3DY, UK. [2]The Gurdon Institute, University of Cambridge, Tennis Court Road, Cambridge CB2 1QN, UK.
[3]These authors contributed equally to the work.
[4]Correspondence should be addressed to B.S. or, if regarding CALI, to B.M. (e-mails: bs251@cam.ac.uk; bm343@cam.ac.uk).

Received 10 July 2009; accepted 12 November 2009; published online 6 December 2009; DOI: 10.1038/ncb2005

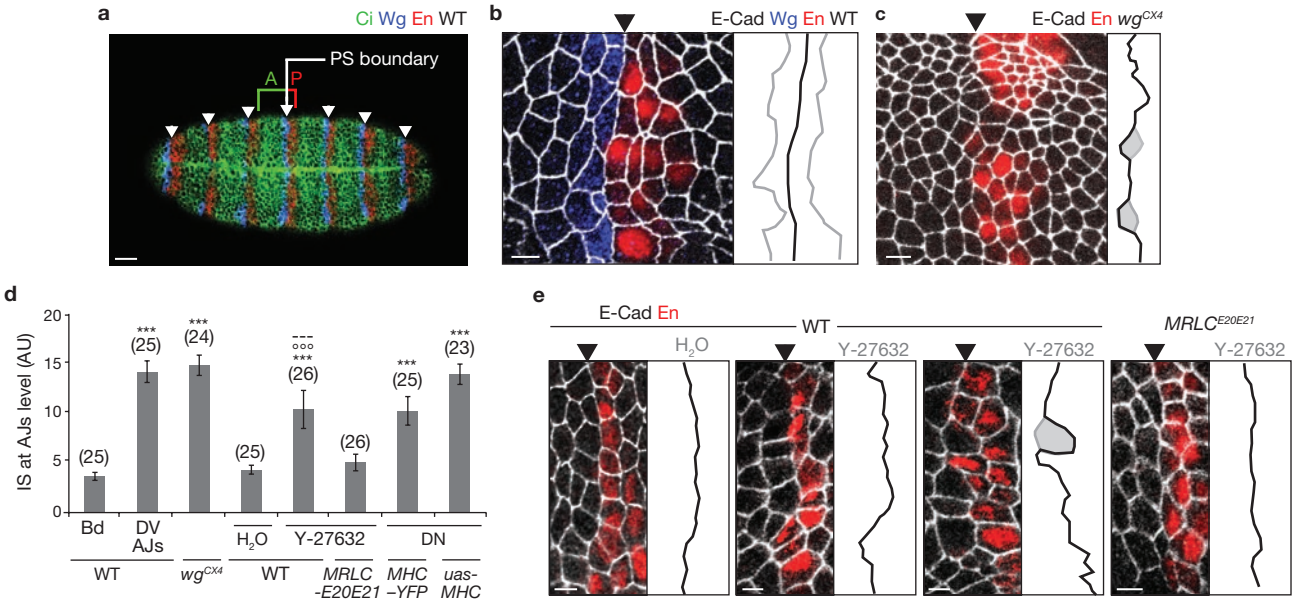

Figure 1 Myosin II is required for cell sorting at lineage restriction boundaries in *Drosophila* embryos. (**a**) Ventral view of an early wild-type *Drosophila* embryo showing expression of Wingless (Wg), Engrailed (En) and Cubitus interuptus (Ci). Parasegmental (PS) boundaries form at the interface between Wg and En stripes (arrowheads), which is where anterior (A) and posterior (P) compartments meet. (**b**) Close-up of the epithelium, with E-Cadherin staining (E-Cad, white) highlighting the adherens junctions. Membrane interfaces at the PS boundary (arrowhead) are arranged in a straight line (black, right panel), in contrast to other columns of interfaces that are not PS boundaries (examples in grey, right panel). (**c**) In a wg^{CX4} mutant embryo, absence of Wg expression leads to loss of En expression and breakdown of compartmentalization. Transient initial En expression allows identification of the membrane interfaces where PS boundaries would have formed (black, right panel): these interfaces are not aligned and some cells (grey, right panel) invade what would have been the neighbouring compartment. (**d**) Index of Straightness (IS, see Methods) quantification confirming that in wild-type embryos, membrane interfaces are straighter at PS boundaries (Bd) compared to non-PS boundaries (DV AJs). PS boundaries lose their straightness in the absence of compartmentalization (wg^{CX4}) or when myosin II (MyoII) function is inhibited by either injection of the drug Y-27632 (see **e**) or expression of dominant-negative constructs (DN, Supplementary Information, Fig. S2). The numbers of boundaries measured are indicated in parentheses (on average, 2–3 boundaries were analysed per embryo). Data are expressed as mean ± s.e.m. Asterisks indicate a statistical comparison with IS at PS boundaries in WT embryos (Student's *t*-test), $***P < 0.001$. Circles and dashes indicate a comparison with WT embryos after H_2O injection, and with $MRLC^{E20E21}$ embryos after Y-27632 injection, respectively. (**e**) In contrast to the control injection of H_2O in WT embryos, injection of Y-27632 (1 mM) led to irregular PS boundaries, with cells occasionally invading the adjacent compartment (grey area). When Y-27632 was injected into embryos expressing $MRLC^{E20E21}$, a phosphomimetic form of MRLC, the boundary defects were fully rescued. Scale bar in **a**, 25 μm, and in **b**, **c** and **e**, 5 μm. WT, wild type. AU, arbitrary units. DV, dorso-ventral. AJ, adherens junction.

did not remove known Wg pathway components, but removed one of the two cytoplasmic *actin* genes (*actin5C*) as well as *spaghetti-squash* (*sqh*), which encodes MRLC (non-muscle myosin II regulatory light chain). To test for a potential role of the actomyosin cytoskeleton in lineage restriction at PS boundaries, we assayed membrane alignment in embryos in which MyoII function was disrupted. Embryos homozygous for null alleles of *zipper*, which encodes the MHC (myosin heavy chain), did not show irregular PS boundaries (data not shown), presumably because maternal pools of MHC are sufficient for its function. To target both maternal and zygotic pools of MyoII, we treated embryos with the drug Y-27632, which inhibits MRLC by preventing its phosphorylation by its upstream activator Rho kinase. Injection of Y-27632 into early embryos, at a dose where the epithelium remained intact and cell divisions were still occuring, disrupted membrane alignment at PS boundaries (Fig. 1d, e; IS = 10.4 ± 1.9, $n = 26$ compared with IS = 4.3 ± 0.4, $n = 25$ in H_2O-injected embryos). The invasion of single cells from anterior or posterior compartments into adjacent compartments was observed (Fig. 1e). PS boundary defects in Y-27632-treated embryos were caused by specific inhibition of MyoII, since these were rescued by expressing a constitutively active phosphomimetic form of MRLC, $MRLC^{E20E21}$, which functions in the absence of Rho kinase (Fig. 1d, e; IS = 5.0 ± 0.8, $n = 26$). Similar cell sorting defects were found in embryos expressing dominant-negative forms of MHC (IS = 10.3 ± 1.4, $n = 25$, for dominant-negative MHC–YFP expressed from an endogenous promoter, and IS = 13.9 ± 1.0, $n = 23$ for upstream activation sequence, UAS, dominant-negative MHC–GFP expressed with *arm*Gal4VP16; Fig. 1d; Supplementary Informaion, Fig. S2). Thus, inhibiting maternal and zygotic pools of MyoII, either by drug injection or by expression of dominant-negative forms of MHC, gives rise to cell sorting defects similar to those caused by loss of anterior/posterior compartmentalization in *wg* mutants. We conclude that a functional actomyosin cytoskeleton is required for lineage restriction at PS boundaries.

To investigate how the actomyosin cytoskeleton controls lineage restriction, we looked at the subcellular organization of filamentous actin and MyoII in boundary cells. MyoII (and to a lesser extent F-actin) is enriched at PS boundary cell–cell interfaces, forming a linear cable-like structure (Fig. 2a; Supplementary Information, Fig. S3a, b), similar to the enrichment reported recently for the wing disc dorsal-ventral boundary[10,11]. We did not observe any difference in the structure of the PS MyoII enrichments between parasegments or between ventral, lateral and dorsal regions of the ectoderm (Supplementary Information, Movie S1; data not shown). Similarly to the planar MyoII enrichment observed at stage 6–8, during germ-band extension[29], both anterior and posterior cells contribute to the

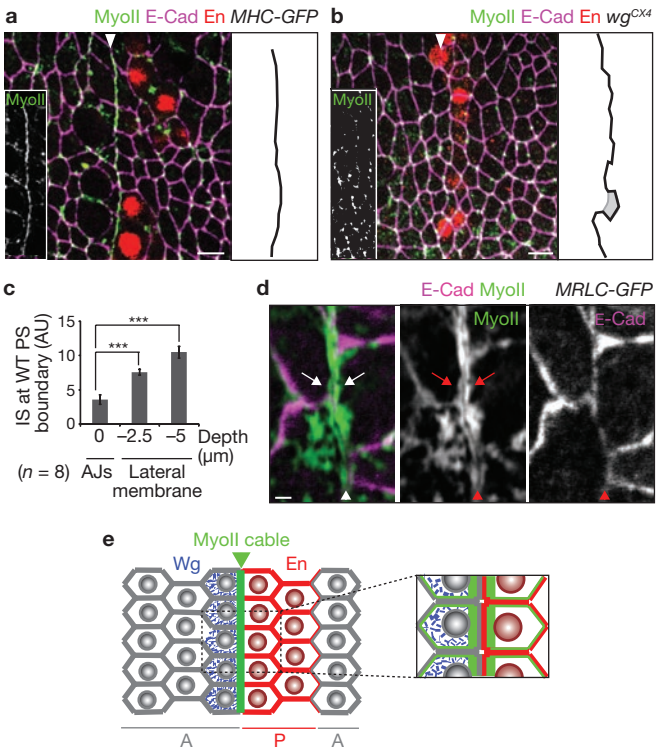

Figure 2 An actomyosin cable forms at the PS boundary. (**a**) Top view of the epidermis showing a confocal section at the level of adherens junctions: MyoII is enriched in a cable-like structure at the membrane interface corresponding to the PS boundary (arrowhead in left panel, black in right panel). (**b**) In the absence of compartmentalization (*wg*^{CX4} embryos), MyoII does not form a cable where PS boundaries would have formed (arrowhead in left panel, black in right panel), but MyoII localization to adherens junctions is unaffected. Grey area in right panel indicates invasion of a cell in what would have been a neighbouring compartment. Insets in **a** and **b** show MyoII staining alone. (**c**) IS at PS boundaries along the apical-basal axis in wild-type embryos: membranes are aligned at the adherens junctions, but lose their alignment 2.5 and 5 μm basal to the adherens junctions ($n = 8$). Data are expressed as mean ± s.e.m. Asterisks indicate a statistical comparison between IS measured at the level of adherens junctions and at the level of the lateral membranes (paired Student's *t*-test), $***P < 0.001$. (**d**) Magnified view of the PS boundary in *MRLC–GFP* embryos: MyoII is enriched at the cortex of both anterior and posterior boundary cells (white and red arrows), on either side of the two apposed plasma membranes labelled by E-cadherin staining. (**e**) Schematic diagram of MyoII enrichment at a PS boundary showing anterior (A) and posterior (P) compartments. Scale bars in **a** and **b**, 5 μm, and in **d**, 1 μm. WT, wild type. AU, arbitrary units. Aj, adherens junction.

PS MyoII cable, as the PS MyoII enrichment is observed at the posterior junction of *wg*-cells and at the anterior junction of *en*-cells (Fig. 2d; Supplementary Information, Fig. S3c). The presence of the PS MyoII cables corresponds to the period of lineage restriction at PS boundaries in wild-type embryos (Supplementary Information, Fig. S3d; stages 8–11). The Myo II cable is located at the level of the adherens junctions (Fig. 2a; Supplementary Information, Fig. S3e, f), which is where membranes are aligned at the PS boundary (IS = 3.6 ± 0.7 at adherens junctions and IS = 10.5 ± 0.9 at 5 μm below adherens junctions, $n = 8$; Fig. 2c, Fig. S3f, g). In addition, the cable is absent in the compartmentalization-mutant *wg*^{CX4} (Fig. 2b). We conclude that lineage restriction at PS boundaries correlates with the presence of a specialized actomyosin structure at the apical cortex of boundary cells (Fig. 2e).

To understand how this cable could promote cell sorting at PS boundaries, we looked at cell behaviours close to the boundaries in live embryos, using MRLC–GFP (Supplementary Information, Movie 1). We found that the PS boundary can be transiently deformed by the division or, more rarely, by the intercalation of boundary cells (Fig. 3a, b; Supplementary Information, Fig. S4a). During these events, the MyoII cable is not dismantled (Fig. 3a, b; Supplementary Information, Fig. S4). When a dividing boundary cell rounds up and transiently invades the adjacent compartment, the MyoII cable at the boundary cortex strongly deforms (Fig. 3c, c′; Supplementary Information, Movie 2). Approximately when cytokinesis starts, the MyoII cable straightens out and the daughter cells go back to their compartment of origin. This suggests that the MyoII cable corrects cell mixing by providing a barrier of cortical tension at boundary interfaces.

To test this hypothesis, we developed a method to specifically inhibit MyoII function in PS boundary cables in live embryos. Chromophore-assisted laser inactivation (CALI) has been used in cultured cells to inactivate single proteins at the subcellular level, including myosins[13,14,30–32]. With CALI, intense laser illumination of a chromophore produces deleterious reactive oxygen species that can inactivate a target protein that is in close proximity (30–45 Å) by cleavage or crosslinking of the peptide backbone[13,33–35]. We modified this method to inhibit MyoII function in live *Drosophila* embryos, using GFP in the MRLC–GFP fusion protein as the target chromophore. In these experiments, MRLC–GFP was expressed in a *sqh*-null background so that each MRLC molecule was tagged with GFP. First, we investigated whether we could inhibit cytokinesis, which requires MyoII function. We found that repeated laser illumination of the MRLC–GFP pool on one side of the ingressing furrow in dividing cells inhibited cytokinesis on that side (Fig. 4a, a′). No inhibition was found in similar experiments targeting Moesin-ABD–GFP, a carboxy-terminal fragment of Moesin fused to GFP, which decorates the actin cytoskeleton but has no function (Fig. 4b, b′). These results show that CALI of MRLC–GFP blocks cytokinesis in live embryos by inhibiting MyoII function at the subcellular level.

To examine the effect of CALI on proteins, we used western blotting to analyse single embryos expressing MRLC–GFP, where a large portion of tissue had been subjected to intense laser illumination (Supplementary Information, Fig. S5a–c). We detected a significant decrease in MRLC–GFP protein levels, whereas levels of associated MHC, or the local membrane-associated protein Dlg, were unaffected. This indicates that the inhibition of MyoII by CALI was caused by destruction of MRLC–GFP. No deleterious effects on cell viability or epithelial integrity were detected (Fig. 4; Supplementary Information, Fig. S5d, d′; data not shown). Together, these results demonstrate that CALI can inhibit MyoII function efficiently and specifically, with resolution at the subcellular level and without detectable cell or tissue toxicity.

We used GFP-based CALI to directly test the requirement of the MyoII cable for cell sorting at PS boundaries. We specifically inhibited the pool of MyoII in the cable by repeated illumination of the PS boundary in *MRLC–GFP*-expressing embryos, and then followed the position of cells by time-lapse imaging of residual GFP fluorescence. We found that when the MyoII cable was inactivated in the presence of dividing boundary cells, the PS boundary was unable to correct cell mixing (100% of cases, $n = 10$), and became irregular (Fig. 5a, d; IS increased from 1.8 ± 0.3 to 9.6 ± 1.0). In these experiments, the pool of MyoII at the cable was the only subcellular pool inactivated, since cytokinesis proceeded normally (Fig. 5e). As

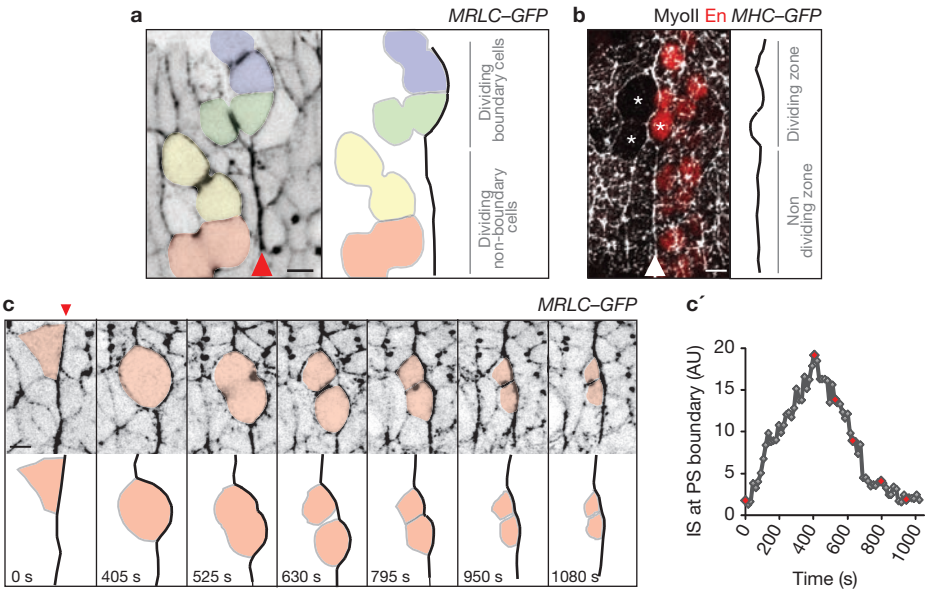

Figure 3 Cell divisions challenge PS boundaries. (**a**) Movie frame showing that dividing boundary cells (coloured blue and green), but not non-boundary cells (coloured red and yellow) deform the MyoII cable at a PS boundary (identified by MRLC–GFP enrichment, arrowhead). (**b**) The MyoII cable (arrowhead) is not dismantled when boundary cells divide (stars). (**c**) Movie frames of a *MRLC–GFP* embryo showing how the division of a boundary cell transiently deforms the MyoII cable (identified by MRLC–GFP enrichment, arrowhead). (**c**´) Quantification of membrane straightness for the first six frames in **c** (red dots). Note that, in contrast to all other quantifications (which consider several boundary cells), the IS measured here corresponds to the length of the interface of the boundary cell/s coloured in red. Scale bars in **a**–**c**, 5 μm.

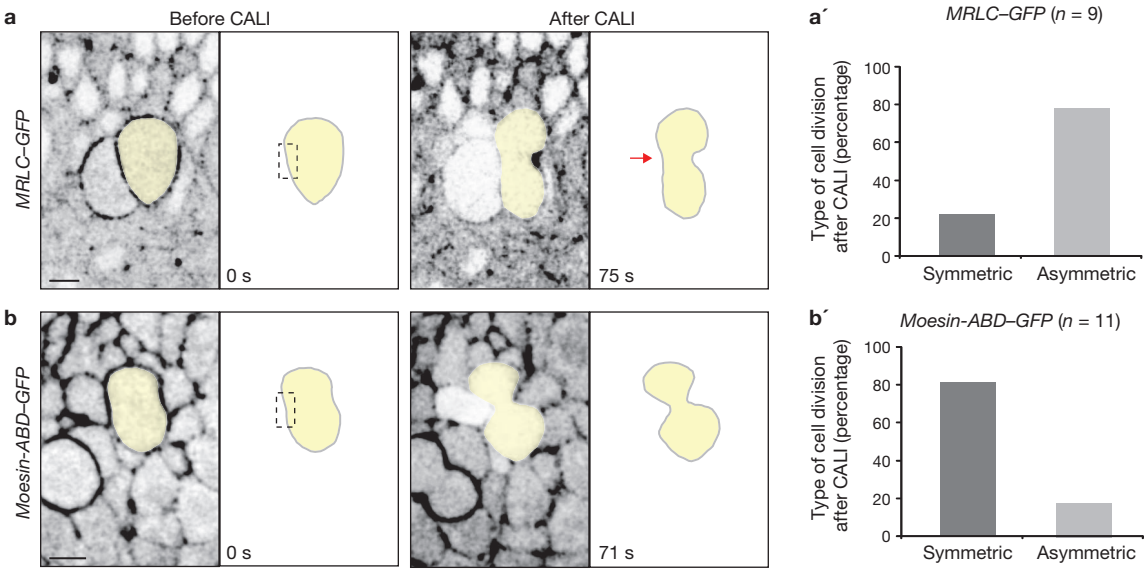

Figure 4 CALI inactivation of MyoII blocks cytokinesis. (**a**, **b**) Movie frames showing that CALI performed on one side (dashed box) of the cytokinesis ring in dividing epithelial cells impairs membrane invagination (red arrow) in *MRLC–GFP* embryos (**a**), but has no effect in *Moesin-ABD–GFP* embryos (**b**). Membrane invagination is impaired in *MRLC–GFP* embryos a few seconds after the beginning of CALI. (**a**´, **b**´) Quantifications of asymmetric (membrane invagination impaired on one side) versus symmetric divisions after CALI in *MRLC–GFP* (**a**´) or *Moesin-ABD–GFP* (**b**´). Scale bars in **a** and **b**, 5 μm.

a control, we used CALI to target Moesin-ABD–GFP at the PS boundary cable and found that this did not affect the boundary in the presence of cell divisions (Fig. 5b, d; IS = 3.4 ± 0.3 before CALI and IS = 3.6 ± 0.5 after CALI, $n = 9$). Since inactivation of MyoII at the cable reproduced the phenotypes found when inhibiting MyoII in the whole tissue, these results suggest that the MyoII cable is responsible for sorting cells at PS boundaries.

We found that the key challenge to embryonic boundaries is the division of boundary cells (Fig. 3a, note that cells dividing at a distance from the boundary had no effect). Consistent with this, CALI inactivation of the MyoII cable in the absence of cell division did not produce cell sorting defects at PS boundaries (Fig. 5c, d; IS = 2.0 ± 0.6 before CALI and IS =2.6 ± 0.3 after CALI in the absence of divisions, $n = 10$, compared with

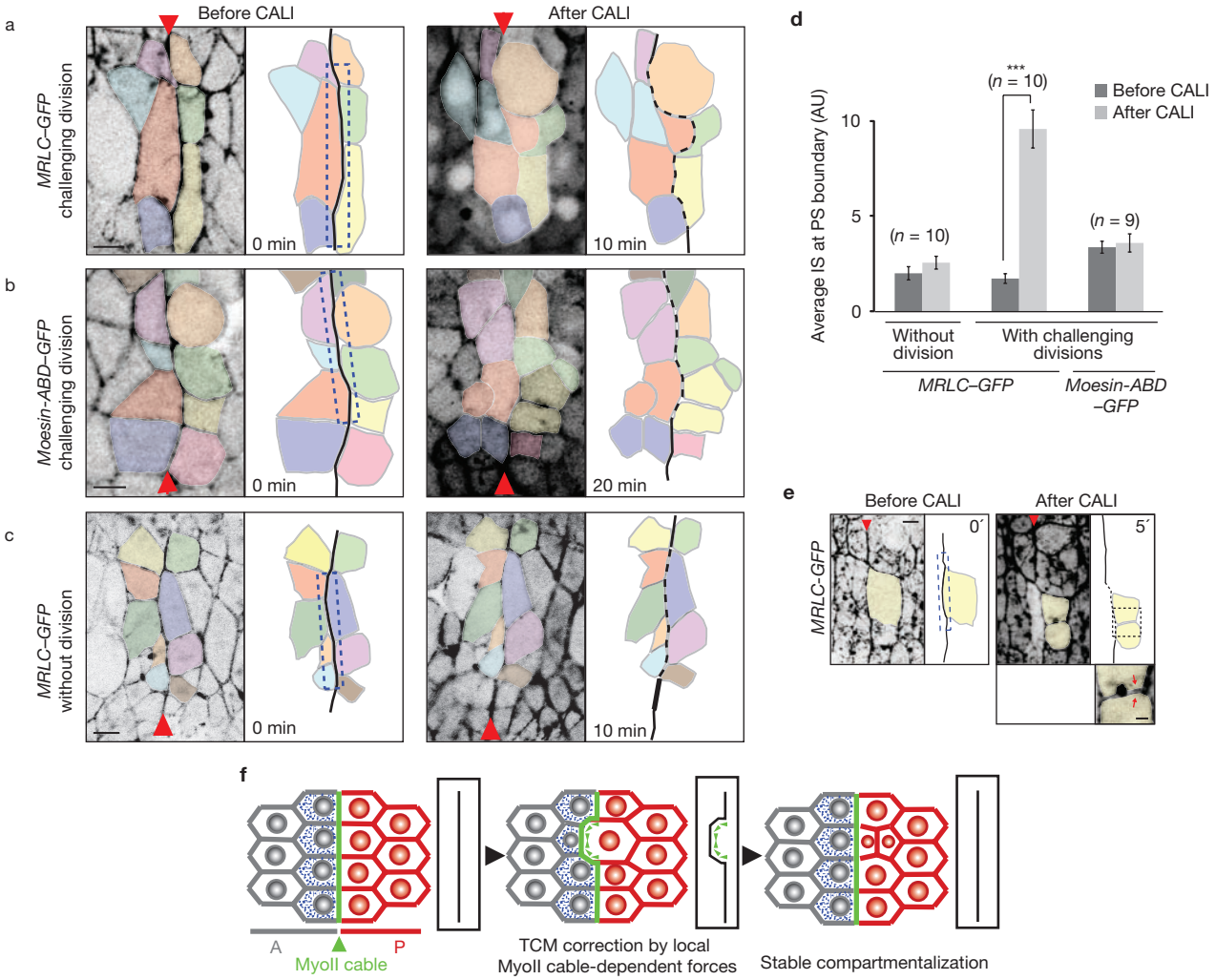

Figure 5 CALI inactivation of the MyoII cable causes cell sorting defects at PS boundaries. (**a**–**c**) Movie frames showing results of CALI on the PS boundary (dashed box) in embryos expressing *MRLC–GFP* (**a**, **c**) or *Moesin-ABD–GFP* (**b**). (**a**) In the presence of a dividing anterior boundary cell (coloured red), CALI inactivation of MyoII at the cable leads to an irregular PS boundary (dashed line, right panel). After division, one daughter cell invades the posterior compartment. (**b**) A similar experiment in *Moesin-ABD–GFP* control embryos does not affect cell sorting at the boundary, even after four of the boundary cells have divided. (**c**) CALI targeting of the MyoII cable in *MRLC–GFP* embryos in the absence of divisions: no cell sorting defects are observed in those conditions. (**d**) Quantification of membrane straightness after CALI at PS boundaries, in the presence or absence of boundary cell divisions. Data are expressed as the mean ± s.em. Asterisks indicate a statistical comparison between conditions before and after CALI in the indicated contexts (paired Student's *t*-test), $***P < 0.001$. (**e**) Cable inactivation (dashed box) does not affect the MyoII pool required for division of the targeted boundary cell (yellow), since the cytokinesis ring forms and the cell divides normally (right panel). Arrows on the close-up view indicate MyoII localizing to the cortex of the newly formed membranes within each daughter cell. (**f**) Model of cell sorting at *Drosophila* embryonic lineage restriction boundaries. TCM, transient cell mixing. Scale bars in **a**–**c**, 5 μm and in **e**, 2 μm. A, anterior compartment. P, posterior compartment.

IS = 1.8 ± 0.3 before CALI and IS = 9.6 ± 1.0 after CALI in presence of divisions, $n = 10$). Moreover, the MyoII cable was present when the embryonic epithelium was mitotically active, and disappeared when divisions ceased in the epidermis (Supplementary Information, Fig. S6). This correlation between mitotic activity and MyoII cabling was also found in the *Drosophila* wing disc. Here, a transient MyoII cable was observed just before the formation of a non-proliferative zone at the wing disc dorso-ventral boundary[10–12] (Supplementary Information, Fig. S6). We propose that actomyosin-based barriers function by generating asymmetric tensile forces at the cortex of challenging boundary cells to prevent them from escaping to the opposite compartment, principally when they divide (Fig. 5f).

In conclusion, our results demonstrate that actomyosin barriers sort cells at compartmental boundaries in the early *Drosophila* embryo. MyoII enrichment at PS boundary interfaces requires Wg signalling (Fig. 2b), however, additional work is required to determine the mechanism involved. One possibility is that *wg*- and *en*-expressing cells have different adhesive properties and that this difference triggers MyoII cabling. In support of this model, mutant clones of the adhesion molecule Echinoid (a Nectin homologue) form actomyosin enrichments at the boundary with wild-type tissue in the *Drosophila* wing disc and follicular epithelium[36,37].

The finding that enrichment of MyoII also occurs at the dorso-ventral compartmental boundaries in the *Drosophila* wing disc[10,11] suggests that assembly of actomyosin-based barriers at boundaries could be a general strategy to stop cells with distinct identities from mixing, especially in mitotically active tissues. In the vertebrate hindbrain, Eph–Ephrin

signalling regulates cell sorting at rhombomeres boundaries[20,21,26]. Given that Eph–Ephrin signalling regulates the actomyosin cytoskeleton in other contexts, such as axonal path finding[38], a role for actomyosin-based barriers could be envisaged in this system.

In developing vertebrate embryos, there is evidence of cell segregation mechanisms not only between compartments, but also between different tissue types[39]. Actomyosin-dependent cortical tension has recently been shown to segregate germ layers in zebrafish[40]. Together with our results, this suggests that local regulation of cortical tension, rather than differential adhesion, could be the primary mechanism behind cell sorting in living organisms. □

Note added in proof: while this paper was in press, a report showed that the cell interfaces at the antero–posterior boundary in the Drosophila *wing disc are under Myosin II-dependent tension. Computational simulations suggested that this increased tension is sufficient for compartmental cell sorting (Landsberg* et al.*, Increased cell bond tension governs cell sorting at the* Drosophila *anteroposterior compartment boundary.* Curr. Biol. *doi:10.1016/j.cub.2009.10.021; 2009).*

METHODS

Methods and any associated references are available in the online version of the paper at http://www.nature.com/naturecellbiology/.

Note: Supplementary Information is available on the Nature Cell Biology website.

ACKNOWLEDGEMENTS

We thank N. Lawrence for the initial observation of the segmental pattern of MyoII cables and for Supplementary Information, Movie 1; B. Bordbar for help in screening chromosomal deficiencies; D. Kiehart, R. Karess, G. Davis, J. Pradel, R. Holmgren, the UK Protein Trap Insertion Consortium, the Bloomington Stock Centre and the Developmental Studies Hybridoma Bank for reagents and B. Harris, R. Keynes, L. Perrin, M. Séméria and D. St Johnston for critical reading of the manuscript. This work was funded by HFSP and Wellcome Trust grants to B.S; a Wellcome Trust Program Grant to A.H.B; an EMBO fellowship to A.P-M and ARC (Association pour la Recherche contre le Cancer) and Herchel Smith fellowships to B.M.

AUTHOR CONTRIBUTIONS

Experimental work and data analysis were carried out by A.P-M and B.M. under supervision of A.H.B. and B.S. All authors contributed to data interpretation and writing of the manuscript.

COMPETING FINANCIAL INTERESTS

The authors declare no competing financial interests.

Published online at http://www.nature.com/naturecellbiology/.
Reprints and permissions information is available online at http://npg.nature.com/reprintsandpermissions/.

1. Dahmann, C. & Basler, K. Compartment boundaries: at the edge of development. *Trends Genet.* **15,** 320–326 (1999).
2. Irvine, K. D. & Rauskolb, C. Boundaries in development: formation and function. *Annu. Rev. Cell Dev. Biol.* **17,** 189–214 (2001).
3. Tepass, U., Godt, D. & Winklbauer, R. Cell sorting in animal development: signalling and adhesive mechanisms in the formation of tissue boundaries. *Curr. Opin. Genet. Dev.* **12,** 572–582 (2002).
4. Dahmann, C. & Basler, K. Opposing transcriptional outputs of Hedgehog signaling and Engrailed control compartmental cell sorting at the *Drosophila* A/P boundary. *Cell* **100,** 411–422 (2000).
5. Garcia-Bellido, A., Ripoll, P. & Morata, G. Developmental compartmentalisation of the wing disk of *Drosophila*. *Nature New Biol.* **245,** 251–253 (1973).
6. Inoue, T. *et al.* Role of cadherins in maintaining the compartment boundary between the cortex and striatum during development. *Development* **128,** 561–569 (2001).
7. Milan, M., Weihe, U., Perez, L. & Cohen, S. M. The LRR proteins Capricious and Tartan mediate cell interactions during DV boundary formation in the *Drosophila* wing. *Cell* **106,** 785–794 (2001).
8. Schlichting, K., Demontis, F. & Dahmann, C. Cadherin Cad99C is regulated by Hedgehog signaling in *Drosophila*. *Dev. Biol.* **279,** 142–154 (2005).
9. Vegh, M. & Basler, K. A genetic screen for hedgehog targets involved in the maintenance of the *Drosophila* anteroposterior compartment boundary. *Genetics* **163,** 1427–1438 (2003).
10. Major, R. J. & Irvine, K. D. Influence of Notch on dorsoventral compartmentalization and actin organization in the *Drosophila* wing. *Development* **132,** 3823–3833 (2005).
11. Major, R. J. & Irvine, K. D. Localization and requirement for Myosin II at the dorsal-ventral compartment boundary of the *Drosophila* wing. *Dev. Dyn.* **235,** 3051–3058 (2006).
12. O'Brochta, D. A. & Bryant, P. J. A zone of non-proliferating cells at a lineage restriction boundary in *Drosophila*. *Nature* **313,** 138–141 (1985).
13. Jacobson, K., Rajfur, Z., Vitriol, E. & Hahn, K. Chromophore-assisted laser inactivation in cell biology. *Trends Cell Biol.* **18,** 443–450 (2008).
14. Jay, D. G. Selective destruction of protein function by chromophore-assisted laser inactivation. *Proc. Natl Acad. Sci. USA* **85,** 5454–5458 (1988).
15. Davy, A., Bush, J. O. & Soriano, P. Inhibition of gap junction communication at ectopic Eph/ephrin boundaries underlies craniofrontonasal syndrome. *PLoS Biol.* **4,** 1763–1776 (2006).
16. Perez-Pomares, J. M. & Foty, R. A. Tissue fusion and cell sorting in embryonic development and disease: biomedical implications. *Bioessays* **28,** 809–821 (2006).
17. Twigg, S. R. *et al.* Mutations of ephrin-B1 (EFNB1), a marker of tissue boundary formation, cause craniofrontonasal syndrome. *Proc. Natl Acad. Sci. USA* **101,** 8652–8657 (2004).
18. Blair, S. S. & Ralston, A. Smoothened-mediated Hedgehog signalling is required for the maintenance of the anterior-posterior lineage restriction in the developing wing of *Drosophila*. *Development* **124,** 4053–4063 (1997).
19. Cheng, Y. C. *et al.* Notch activation regulates the segregation and differentiation of rhombomere boundary cells in the zebrafish hindbrain. *Dev. Cell* **6,** 539–550 (2004).
20. Cooke, J. E., Kemp, H. A. & Moens, C. B. EphA4 is required for cell adhesion and rhombomere-boundary formation in the zebrafish. *Curr. Biol.* **15,** 536–542 (2005).
21. Mellitzer, G., Xu, Q. & Wilkinson, D. G. Eph receptors and ephrins restrict cell intermingling and communication. *Nature* **400,** 77–81 (1999).
22. Milan, M. & Cohen, S. M. A re-evaluation of the contributions of Apterous and Notch to the dorsoventral lineage restriction boundary in the *Drosophila* wing. *Development* **130,** 553–562 (2003).
23. Morata, G. & Lawrence, P. A. Control of compartment development by the engrailed gene in *Drosophila*. *Nature* **255,** 614–617 (1975).
24. Rodriguez, I. & Basler, K. Control of compartmental affinity boundaries by hedgehog. *Nature* **389,** 614–618 (1997).
25. Shen, J. & Dahmann, C. The role of Dpp signaling in maintaining the *Drosophila* anteroposterior compartment boundary. *Dev. Biol.* **279,** 31–43 (2005).
26. Xu, Q., Mellitzer, G., Robinson, V. & Wilkinson, D. G. *In vivo* cell sorting in complementary segmental domains mediated by Eph receptors and ephrins. *Nature* **399,** 267–271 (1999).
27. Sanson, B. Generating patterns from fields of cells: examples from *Drosophila* segmentation. *EMBO Rpts* **2,** 1083–1088 (2001).
28. Vincent, J. P. & O'Farrell, P. H. The state of engrailed expression is not clonally transmitted during early *Drosophila* development. *Cell* **68,** 923–931 (1992).
29. Zallen, J. A. & Wieschaus, E. Patterned gene expression directs bipolar planar polarity in *Drosophila*. *Dev. Cell* **6,** 343–355 (2004).
30. Rajfur, Z., Roy., P., Otey, C., Romer, L. & Jacobson, K. Dissecting the link between stress fibres and focal adhesions by CALI with EGFP fusion proteins. *Nature Cell Biol.* **4,** 286–293 (2002).
31. Diefenbach, T. J. *et al.* Myosin 1c and myosin IIB serve opposing roles in lamellipodial dynamics of the neuronal growth cone. *J. Cell Biol.* **158,** 1207–1217 (2002).
32. Wang, F. S., Wolenski, J. S., Cheney, R. E., Mooseker, M. S. & Jay, D. G. Function of myosin-V in filopodial extension of neuronal growth cones. *Science* **273,** 660–663 (1996).
33. Horstkotte, E., Schroder, T., Niewohner, J., Jay, D. G. & Henning, S. W. Toward understanding the mechanism of chromophore-assisted laser inactivation - evidence for the primary photochemical steps. *Photochem. Photobiol.* **81,** 358–366 (2005).
34. Liao, J. C., Roider, J. & Jay, D. G. Chromophore-assisted laser inactivation of proteins is mediated by the photogeneration of free-radicals. *Proc. Natl Acad. Sci. USA* **91,** 2659–2663 (1994).
35. Yan, P. *et al.* Fluorophore-assisted light inactivation of Calmodulin involves singlet-oxygen mediated cross-linking and methionine oxidation. *Biochemistry* **45,** 4736–4748 (2006).
36. Laplante, C. & Nilson, L. A. Differential expression of the adhesion molecule Echinoid drives epithelial morphogenesis in *Drosophila*. *Development* **133,** 3255–3264 (2006).
37. Wei, S. Y. *et al.* Echinoid is a component of adherens junctions that cooperates with DE-Cadherin to mediate cell adhesion. *Dev. Cell* **8,** 493–504 (2005).
38. Huber, A. B., Kolodkin, A. L., Ginty, D. D. & Cloutier, J.-F.o. Signaling at the growth cone: ligand–receptor complexes and the control of axon growth and guidance. *Ann. Rev. Neurosci.* **26,** 509–563 (2003).
39. Townes, P. L. & Holtfreter, J. Directed movements and selective adhesion of embryonic amphibian cells. *J. Exp. Zool.* **128,** 53–120 (1955).
40. Krieg, M. *et al.* Tensile forces govern germ-layer organization in zebrafish. *Nature Cell Biol.* **10,** 429–436 (2008).

DOI: 10.1038/ncb2005

METHODS

Fly strains. *yw* was used as a wild type. The following transgenes were used: *sqh*^{AX3}; *sqh>sqhGFP42* (*MRLC–GFP*)[41], Cyo, *zip*$^{WeeP181-GFP}$ (*MHC–GFP*)[42], *sqh>MoesinABD–GFP* (*Moe-ABD–GFP*, also known as *sGMCA*)[43], *MRLC*^{E20E21} (phosphomimetic form of MRLC)[44]; *en*>Gal4 (ref. 45), *wg*>Gal4 (a gift from J. Pradel, Developmental Biology Institute of Marseilles, France), *arm*>FRT-stop-FRT-Gal4VP16 (ref. 46); KB19 (male specific flipase)[46]; UAS>*GFP–MHC*[47], UAS>*GFP–DN-MHC*[47]. The following null mutant alleles were used: *wg*^{CX4} (ref. 48), *zip*$^{1.3}$ (ref. 49), *zip*^{1} (ref. 50) and *zip*^{2} (ref. 50). *zip*$^{CPTI-100026}$ (*DN-MHC-YFP*) is a new allele of *zipper* (it does not complement *zip*^{1}, *zip*^{2} *and zip*$^{1.3}$), which possesses a YFP exon inserted in the head domain of MHC (line from the UK Protein Trap Insertion Consortium, D. St Johnston, K. Lilley and S. Russell, unpublished). This allele behaves as a dominant negative.

Deficiency screen. The deficiency screen was performed using the molecularly mapped Drosdel chromosomal deficiencies[51]. Stage 9–11 embryos were stained using an anti-En antibody and revealed with an anti-mouse-HRP secondary antibody (Jackson laboratory, 1:200) and DAB staining. Embryos were analysed under a Zeiss Axioplan 2 microscope, and were screened for an irregular arrangement of En nuclei at PS borders.

Immunostainings and antibodies. Embryos were fixed for 5 min in heptane: formaldehyde 37% (1:1). For E-cadherin and F-actin, and generally MyoII, embryos were devitellinised manually and stained immediately. Primary antibodies obtained from DSHB were: Mouse anti-Wg (4D4; 1:50), anti-En (4D9; 1:100), anti-Nrt (BP106; 1:5) anti-Dlg (4F3; 1:500) and rat anti-DE-cadherin (DCAD2; 1:50). Other primary antibodies were: rat anti-Ci (2A1; 1:3; ref. 52), mouse anti-GFP (cat.#11-814-460-001, Roche; 1:50), rabbit anti-En (d300, Santa Cruz Biotechnology, inc.; 1:100) and rabbit anti-GFP (ab6556, Abcam; 1:500). Secondary antibodies: were either conjugated to Alexa fluorochromes (Alexa 488, Alexa 564 or Alexa 633) and used at a 1:500 dilution or to Jackson fluorochromes (TRITC or Cy5) and used at a 1:200 dilution. F-actin was stained using phalloidin-Alexa 546 (Molecular probes; 1:1,000)

Live imaging. Dechorionated embryos were immobilised on a coverslip with heptane glue and immersed in Voltalef oil (ELF Atochem). Live imaging was performed with a Zeiss LSM510 inverted confocal with 40× or 63× objectives. Projections of *z*-stack images were used to generate movies with Image J software.

Quantification of membrane straightness and assessment of compartmental cell mixing. The index of straightness (IS) was calculated as the difference between measured and minimal theoretical length between two points after normalization, and was expressed in arbitrary units (AU). A value of 1 AU meant that the measured length was 1% longer than the straight line. Membrane length was measured using Image J software. The length of membrane interfaces for PS boundary cells or for other columns of cells was measured in the absence of cell division (except for Fig. 3c′).

In fixed embryos, membrane interfaces corresponding to PS boundaries were identified by En expression. Measurements were performed on confocal sections corresponding to the plane of the adherens junctions. Images were captured at random locations along anterior/posterior and dorso-ventral axes in the embryo trunk, using a 40× objective and a numerical zoom 4 on a Zeiss LSM510 confocal microscope. The images shown correspond to a superposition of E-cadherin staining at the adherens junctions (usually one confocal section) and a projection of all *z* sections for En staining. Note that the whole stack of *z* sections in these double stainings were systematically checked to accurately identify the interfaces corresponding to the PS boundary.

In live embryos, including in CALI experiments, PS boundaries were identified by MyoII or Moesin-ABD–GFP enrichment. Images were taken with a 63× objective and a numerical zoom 3 on a Zeiss LSM510 confocal microscope.

In experimental cases where the PS boundary was irregular compared with that in wild-type embryos, some cells were displaced into the adjacent compartment. These events were considered to be compartmental cell mixing when the displaced cell had less junctional contacts with cells of the same identity than with cells of a different identity.

Injection of the ROCK inhibitor Y-27632. Stage 8–9 embryos of the indicated genotype were injected in the yolk at room temperature with 1 mM Y-27632 (TOCRIS) or dH_2O in control experiments. Embryos were aged for 30 min at 25 °C, fixed and stained using standard procedures.

As loss of epithelial integrity leads to massive cell dispersal in the early *Drosophila* embryo[53], epithelial integrity was systematically checked using E-cadherin staining in loss-of-function experiments. The highest concentration of Y-27632 that can be used without affecting epithelium integrity is 1 mM, and at this concentration some cell divisions still occur.

Western blots of single embryos and quantification of protein levels. Two protocols were used for western blotting: one included a fixation step for GFP and Phospho-MRLC, and the other did not include fixation for MHC. GFP and Dlg work in both conditions. Single embryos glued on a coverslip were detached by soaking them briefly in heptane. If fixation was required, embryos were transferred to fixative solution (formaldehyde 37%: heptane (1:1)) and fixed for 5 min, thoroughly rinsed with PBS 1X Triton X-100 0.1% and hand devitellinised in PBS. Embryos (5–10) were pooled in 100–200 µl of Laemli buffer: PBS 1X (1:1) and boiled for 5 min. When fixation was not required, embryos were thoroughly rinsed with PBS 1X Triton X-100 0.1%, transferred to 20 µl of Laemli buffer: PBS 1X (1:1), carefully crushed with a needle and boiled for 5 min.

The equivalent of one embryo was loaded per lane. Standard procedures were used for western blotting analysis. Revelation was performed using ECL Standard Plus kit (Perkin Elmer Life Science). Primary antibodies used were: mouse anti-Dlg (DSHB; 1:300) and anti-GFP (Roche; 1:500), rabbit anti-Phospho-MRLC (Phospho-Ser19; cat.#3671, CST; 1:100,) and anti-MHC (#656, 1:10,000; ref. 54). Secondary antibodies used were: mouse or rabbit HRP-conjugated (Jackson Laboratories; 1:2,000).

Films were scanned and quantification of protein level**S** was performed using Image J software. Since there is no significant difference in Dlg protein levels between control and CALI-treated embryos ($n = 13$; which is consistent with Dlg being unaffected when examining immunofluorescence levels in whole embryos; Supplementary Information, Fig. S5d, d′), Dlg was used as a loading control to normalize protein levels for GFP, phospho-MRLC and MHC.

Statistical analyses. Data from all quantifications are reported as mean ± s.e.m. The significance between groups of data was assessed by unpaired Student's *t*-test (Fig.1d) or by paired Student's -test (Fig.1d, boundary vs dorso-ventral junctions in wild type; Figs 2c, 5d; Supplementary Information, Fig. S5b). Results were considered significant when $P < 0.05$ ($^{*}P < 0.05$, $^{**}P < 0.02$, $^{***}P < 0.001$).

Chromophore-assisted laser inactivation (CALI). GFP was used as a chromophore to perform CALI on two fusion proteins, MRLC–GFP[41] and the control Moesin-ABD–GFP[43]. MRLC–GFP was used in a null background mutant for *spaghetti-squash*. The control Moesin-ABD–GFP, which corresponds to the actin-binding domain of Moesin that decorates F-actin, was expressed in a wild-type background. CALI was performed using either an inverted or an upright LSM510 laser-scanning confocal microscope (Zeiss) with a Lasos 50 mW argon laser set at 50% of its power. For image acquisition, GFP was excited using the 488-nm laserline at 1–3%. For CALI itself, to excite GFP maximally and hence to locally produce maximum levels of reactive oxygen species, both 477-nm and 488-nm laserlines set at 100% were used. Depending on the experiment, we used a Plan-Apochromat 63×/1.4 Oil DIC objective or a Plan-Neofluar 40×/1.3 Oil DIC objective (Zeiss).

CALI conditions for assessment of protein integrity by western blotting and immunostaining. CALI was performed during dorsal closure on the dorsal side of *MRLC–GFP* embryos by continuously scanning a region of interest (ROI) for 5 min. Protein levels were then analysed by western blotting or whole-mount immunostaining. For western blotting analysis, we used a 63× objective and a ×0.7 numerical zoom. We scanned a ROI of 200 µm × 120 µm (which roughly covers the trunk of the embryo) to a depth of 21 µm (15 sections every 1.5 µm). Parameters were: pixel time, 12.8 µs; scan time, 798.91 ms; scan speed, 5 arbitrary units; number of scans per frame, 1; pinhole, 3.37 airy units. For immunostaining analysis, we used a 40× objective and a ×0.7 numerical zoom. We scanned a ROI of 90 µm × 50 µm to a depth of 12 µm (9 sections every 1.5 µm). Parameters were: pixel time, 6.39 µs; scan

time, 552.44 ms; scan speed, 6 arbitrary units; number of scans per frame, 2; pinhole, 0.93 airy unit. As soon as CALI was completed, embryos were individually processed for western blotting or immunostaining experiments (see above).

CALI conditions for MyoII inhibition during cytokinesis. CALI was performed on ectodermal dividing cells on stage 9–10 *MRLC–GFP* (or *Moesin-ABD–GFP)* embryos using a 40× objective and a ×5 numerical zoom. We used laser pulses (6–8 s) followed by acquisition of ten images (1 per s). Parameters, based on the LSM510 Frap module (Zeiss), were: pixel time, 1.60 µs; scan speed, 9 arbitrary units; number of scans per frame, 1; pinhole, 0.93 airy unit; iterations, 10. The cytokinesis ring was targeted at only one focal plane with an average ROI of 5 µm × 2 µm. When required, the ROI was slightly shifted during the experiment to follow the cytokinesis ring. The opposite side of the cytokinesis ring was used as an internal control.

CALI conditions for MyoII inhibition at the PS cable. CALI was performed on stage 9 to early stage 10 *MRLC–GFP* (or *Moesin-ABD–GFP*) embryos using a 63× objective and a ×3 numerical zoom. A cycle (1 laser pulse + 1 acquisition) lasted 6–9 seconds, depending of the ROI size. The PS boundary was targeted at only one focal plane with a ROI of 3 µm × 20 µm on average. When required, the ROI was slightly shifted in the *x*, *y* and/or *z* axis during the experiment, to follow the PS boundary. CALI was performed for 1–10 min on boundary cells before division. Parameters, based on the LSM510 Frap module (Zeiss), were: pixel time, 2.56 µs; scan speed, 8 arbitrary units; number of scans per frame, 1; pinhole, 3.37 airy units; iterations, 3. One image was aquired before each CALI experiment and was used as a reference. During and after CALI, cells were tracked by time-lapse microscopy using residual GFP fluorescence. Modification of membrane straightness was measured only in the targeted area, at the adherens junctions level and when challenging divisions were completed.

41. Royou, A., Sullivan, W. & Karess, R. Cortical recruitment of nonmuscle myosin II in early syncytial *Drosophila* embryos: its role in nuclear axial expansion and its regulation by Cdc2 activity. *J. Cell Biol.* **158,** 127–137 (2002).
42. Clyne, P. J., Brotman, J. S., Sweeney, S. T. & Davis, G. Green fluorescent protein tagging *Drosophila* proteins at their native genomic loci with small P elements. *Genetics* **165,** 1433–1441 (2003).
43. Kiehart, D., Galbraith, C., Edwards, K., Rickoll, W. & Montague, R. Multiple forces contribute to cell sheet morphogenesis for dorsal closure in *Drosophila*. *J. Cell Biol.* **149,** 471–490 (2000).
44. Winter, C. G. *et al. Drosophila* Rho-associated kinase (Drok) links Frizzled-mediated planar cell polarity signaling to the actin cytoskeleton. *Cell* **105,** 81–91 (2001).
45. Brand, A. H. & Perrimon, N. Targeted gene expression as a means of altering cell fates and generating dominant phenotypes. *Development* **118,** 401–415 (1993).
46. Sanson, B., White, P. & Vincent, J. P. Uncoupling cadherin-based adhesion from wingless signalling in *Drosophila*. *Nature* **383,** 627–630 (1996).
47. Franke, J., Montague, R. & Kiehart, D. Nonmuscle Myosin II generates forces that transmit tension and drive contraction in multiple tissues during dorsal closure. *Current Biology* **15,** 2208–2221 (2005).
48. Baker, N. E. Molecular cloning of sequences from wingless, a segment polarity gene in *Drosophila*: the spatial distribution of a transcript in embryos. *EMBO J.* **6,** 1765–1773 (1987).
49. Young, P. E., Richman, A. M., Ketchum, A. S. & Kiehart, D. P. Morphogenesis in *Drosophila* requires nonmuscle myosin heavy chain function. *Genes Dev.* **7,** 29–41 (1993).
50. Tearle, R. G. & Nusslein-Volhard, C. Tübingen mutants and stock list. *Dros. Inf. Serv.* **66,** 209–269 (1987).
51. Ryder, E. *et al.* The DrosDel deletion collection: a *Drosophila* genomewide chromosomal deficiency resource. *Genetics* **177,** 615–629 (2007).
52. Motzny, C. K. & Holmgren, R. The *Drosophila* cubitus interruptus protein and its role in the wingless and hedgehog signal transduction pathways. *Mech. Dev.* **52,** 137–150 (1995).
53. Chandraratna, D., Lawrence, N., Welchman, D. P. & Sanson, B. An *in vivo* model of apoptosis: linking cell behaviours and caspase substrates in embryos lacking DIAP1. *J. Cell Sci.***120,** 2594–2608 (2007).
54. Kiehart, D. P. & Feghali, R. Cytoplasmic myosin from *Drosophila melanogaster*. *J. Cell Biol.* **103,** 1517–1525 (1986).

nature cell biology

DOI: 10.1038/ncb2005

In all supplementary figures, genotypes are italicised and proteins are capitalised. Unless indicated, embryos are late stage 9-early stage 10, with anterior to the left. Top views are shown except indicated and scale bars represent 5 μm. PS boundaries are indicated by arrowheads.

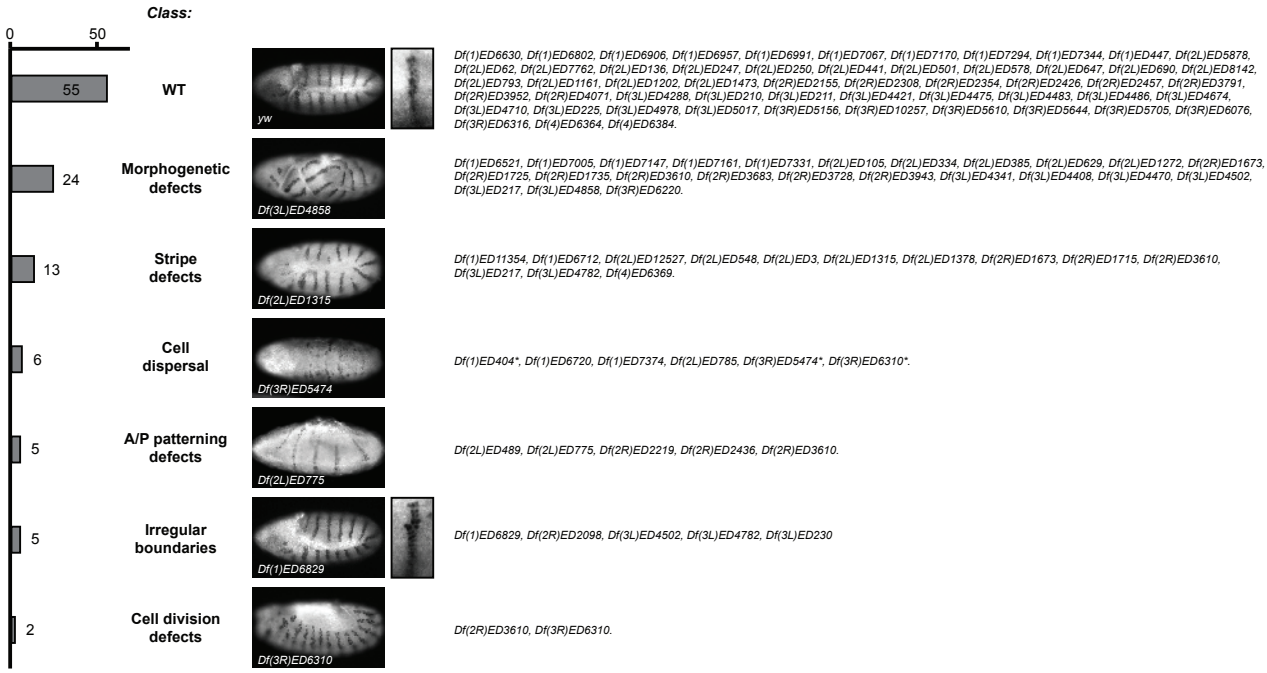

Figure S1 A deficiency screen for altered Engrailed expression patterns. 102 molecularly characterised chromosomal deficiencies from Drosdel have been analysed by Engrailed (En) immunostaining. Phenotypes fall into seven classes. For each class, one representative image is given, as well as the number (left) and the full list of deficiencies showing this class of phenotype. Note that a few deficiencies are annotated in several classes. Deficiencies annotated as "Morphogenetic defects" present one or several of the following defects: twisted embryos (illustrated), ventral closure defects, aberrant cephalic furrow, germ-band extension defects, irregular distance between stripes or larger head region. Deficiencies annotated as "Stripe defects" present one or several of the following defects: interrupted stripes (illustrated), missing stripes, fused stripes, wide stripes. Deficiencies annotated as "Cell dispersal" present extensive dispersal of *en*-expressing cells, reminiscent of the "salt and pepper" phenotype caused by loss of DIAP1 function described by Chandraratna et al[1]. In that case, loss-of-function of DIAP1 leads to premature death of all cells, with loss of epithelial integrity and cell dispersal[1]. The symbol * indicates deficiencies for which premature cell death has been confirmed using a TUNEL assay. Deficiencies annotated as "AP patterning defects" correspond to loss of *engrailed* expression, pair rule-like (illustrated) or gap-like phenotypes. Deficiencies annotated as "Irregular boundaries" present irregular parasegmental boundaries. *Df(1)ED6829* (illustrated) removes both *actin5c* and *spaghetti squash*, the gene coding for the Myosin Regulatory Light Chain. Three deficiencies remove genes that modify Wingless signalling or expression: *broken heart (Df(2R)ED2098)*, *naked cuticle* and *frizzled2 (Df(3L)ED4782); Tenascin*-M *(Df(3L)ED230)*. Deficiencies annotated as "Cell division defects" present fewer cells with larger nuclei. Molecular coordinates, cytology and the list of genes deleted for each deficiency can be obtained at http://www.drosdel.org.uk/.

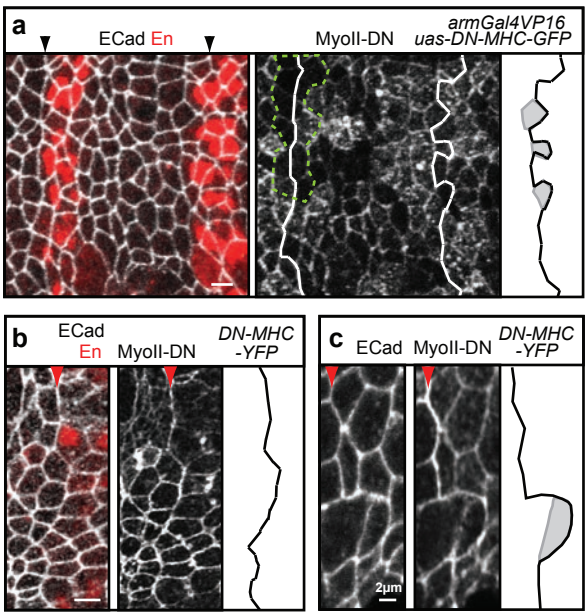

Figure S2 Inhibition of Myosin II by dominant-negative constructs causes cell sorting defects at PS boundaries**.** (a-c) PS boundaries where MyoII activity has been impaired by expression of dominant negative forms of Myosin Heavy Chain: UAS-DN-MHC-GFP (a) and DN-MHC-YFP (b, c). In both experiments, PS boundaries become irregular and some boundary cells invade the adjacent compartment (highlighted in grey). In a, variable levels of expression with armGal4VP16 reveal that the strength of these phenotypes correlates with dominant-negative forms expression levels. Weak expression of UAS-DN-MHC-GFP in PS boundary cells correlates with a straight boundary (second panel, left-hand side boundary), whereas strong expression in other PS boundary cells correlates with an irregular boundary (right-hand side boundary). Also, UAS-DN-MHC-GFP expression using the UAS-Gal4 system is in average higher than DN-MHC-YFP expression, which depends upon the MHC endogeneous promoter. Measurements of PS boundary interfaces straightness reflect this difference (see quantification in Fig. 1d).

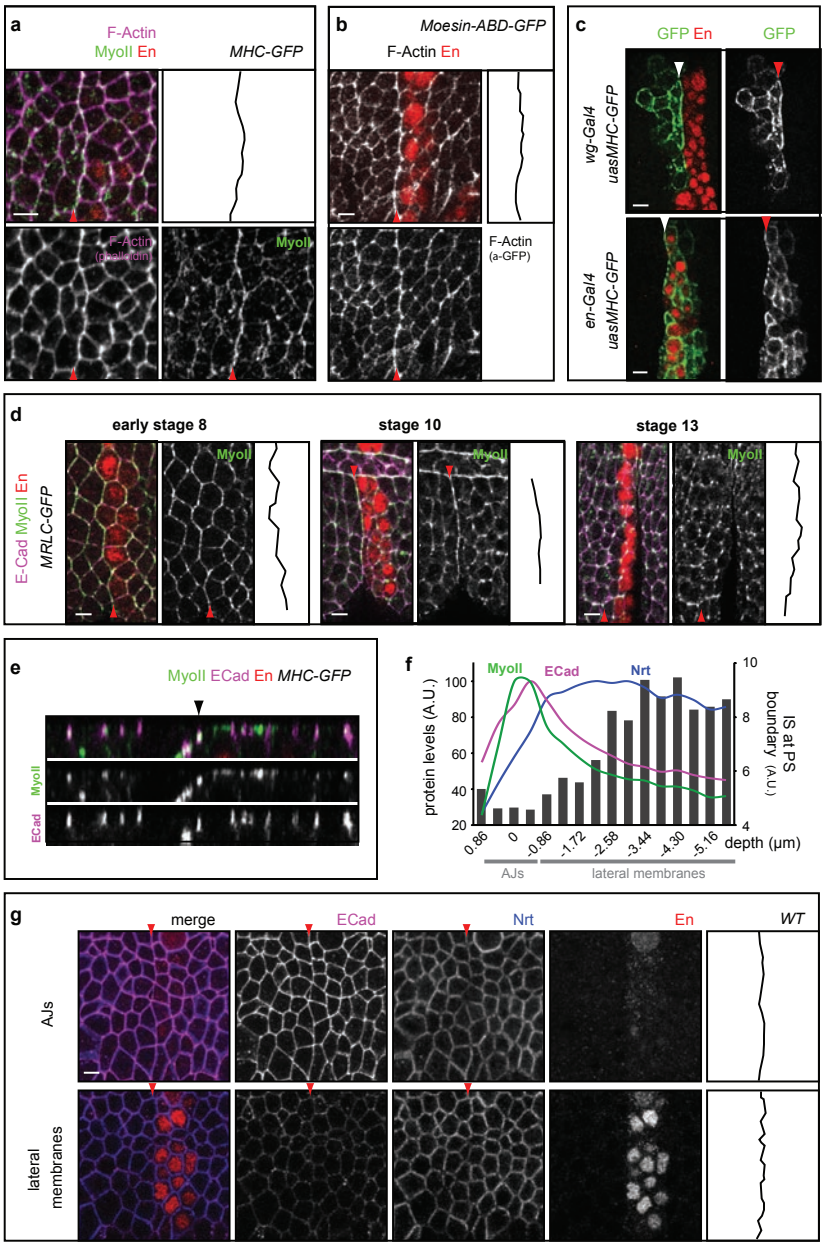

Figure S3 Description of the actomyosin PS cable. (a, b, d) Both MyoII components (Myosin Heavy Chain in a; Myosin Regulatory Light Chain in d) and the actin cytoskeleton (F-actin in a; Moesin-ABD-GFP in b) are enriched at PS boundaries. MyoII and F-Actin enrichments colocalise at the PS boundary (a), forming a cable-like structure that connects all the boundary cells. (c) Expression of MHC-GFP in the anterior *wg*-expressing cells or in the posterior *en*-expressing cells both reveal the MyoII cable at PS boundaries, showing that MyoII is enriched at the cortex of both anterior and posterior cells. (d) MyoII enrichment at PS boundaries correlates temporally with the period of lineage restriction in early embryos (i.e. stages 8-11[2]). Triple staining for MyoII (green), ECad (purple) and En (red) at different stages of embryonic development shows that MyoII starts to be enriched at PS boundaries at early stage 8 (arrowhead in left panel). Note that the boundary is not straight yet. A strong MyoII enrichment is detected from late stage 8 to stage 11 at PS boundaries (arrowhead in middle panel), which correlates with the presence of parasegmental grooves (indentation at the bottom of panel). By stage 12, MyoII cables start to be dismantled, so no enrichment can be detected by stage 13 at the interfaces corresponding to the anterior border of the Engrailed cells (arrowhead in right panel). The PS groove has disappeared, and the segmental groove has formed on the posterior side of the En stripe. (e) Lateral view of the epithelium (XZ confocal cross-section of Fig. 2a) showing that MyoII and ECad colocalise. Note that the adherens junctions (AJs) are slightly more basal at the PS boundary, which is consistent with the subtle indentations called parasegmental grooves that mark PS boundaries in early embryos[3, 4] (Immediately left to the PS adherens junctions are a cluster of more basal E-CAD and MyoII stainings: these correspond to a cell which had rounded up prior to division, see top view in Fig. 2a). (f) Quantification of the membrane interfaces straightness (IS, bars) relative to E-Cad, MyoII and Neurotactin (Nrt) protein levels at a PS boundary. Membrane interfaces are straight at the level of AJs (maximal intensity of E-Cad staining) and this correlates with the position of the MyoII cable (maximal intensity of MyoII staining). Nrt is a marker of lateral membranes. (g) Confocal views of the epidermis corresponding to an optical section at the level of the AJs (top panels) or 5 μm below (bottom panels). Membrane interfaces are straight at the PS boundary at AJs level, but become irregular in the more basal section.

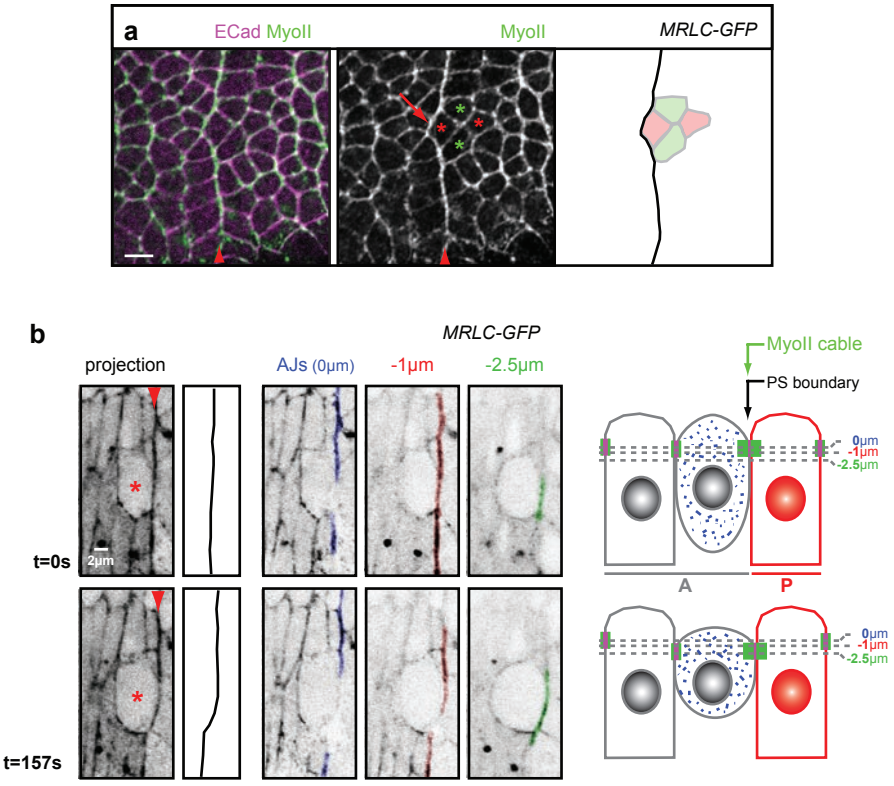

Figure S4 The MyoII cable at PS boundaries is maintained when boundary cells divide or intercalate. (a) Boundary cells (arrow) which belong to cell intercalation figures[5] (stars, extracted in red and green) do not dismantle the MyoII cable and deform the PS boundary. (b) Movie frames showing a boundary cell rounding up prior to division (star) in a *MRLC-GFP* embryo. Left-hand side panels show a projection of 3 confocal sections displayed separately on the right-hand side panels, with the PS MyoII cable highlighted in blue (section at AJs level), red (section 1 µm below) and green (section 2.5 µm below). The MyoII cable is not dismantled but become more basal as the rounding up boundary cell adopts a more basal position: the MyoII cable is visible in the -1µm section at time 0 and in the -2.5 µm section 157 seconds later.

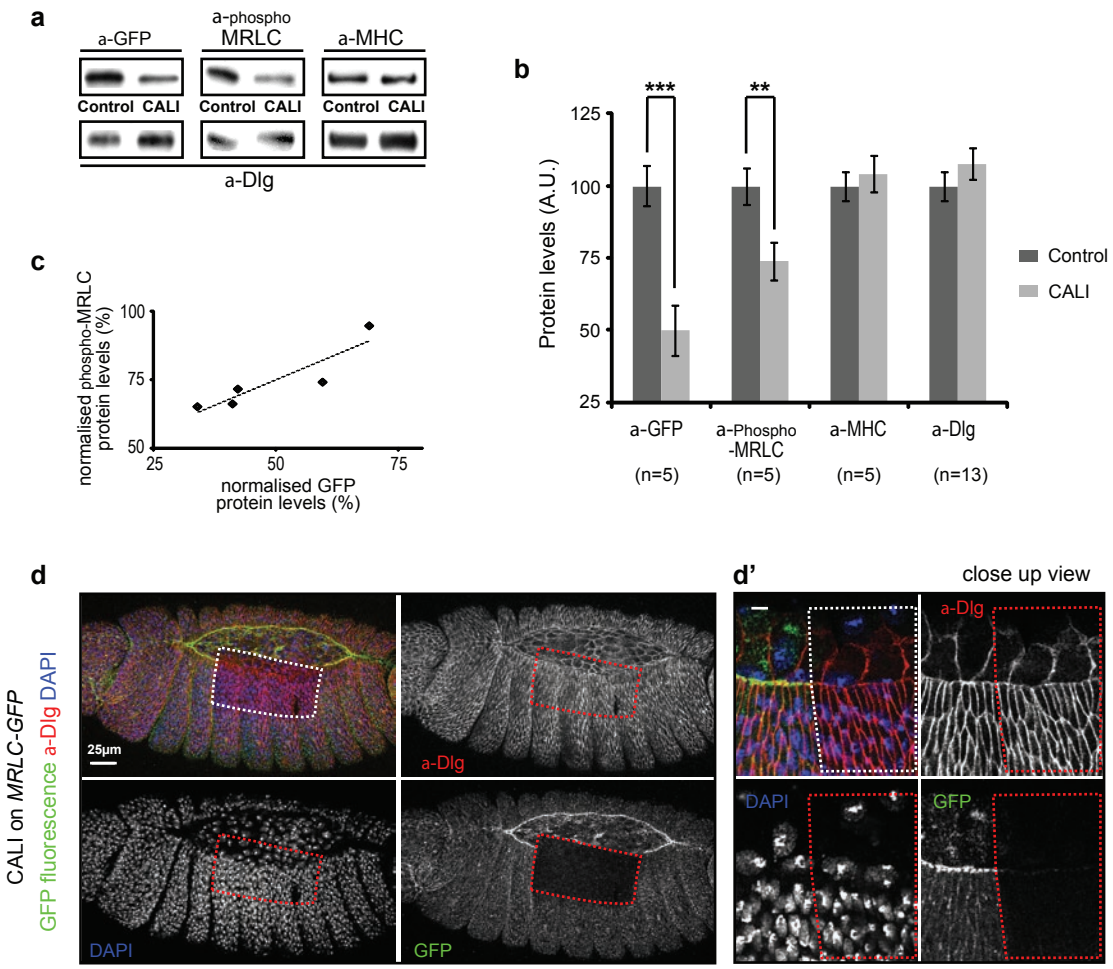

Figure S5 CALI on MRLC-GFP decreases specifically GFP and MRLC protein levels. (a-c) Analysis of protein levels in *MRLC-GFP* embryos illuminated by laser over the dorsal part of their trunk to promote widespread CALI. (a) Western blots of single embryos extracts show that levels of GFP and phospho-MRLC are decreased after CALI, whereas associated MHC and nearby membrane protein Dlg levels are unaffected. (b) Quantifications of protein levels in control or CALI targeted embryos based on Western blots. Data are expressed as mean ± SEM and compared with paired Student's t test. P Values: ** correspond to p<0.02 and *** to p<0.001. (c) There is a linear relationship between the decrease in GFP and phospho-MRLC protein levels following CALI (points represent the individual experiments averaged in b). (d,d') CALI performed on the dorsal side of *MRLC-GFP* embryos (dashed box) during dorsal closure (stage 14) does not affect the epithelium's structure, as revealed by staining membranes with Dlg (red) and nuclei with DAPI (blue). The region targeted by CALI is identified by the loss of GFP fluorescence (green). d' shows a high magnification of the epithelium.

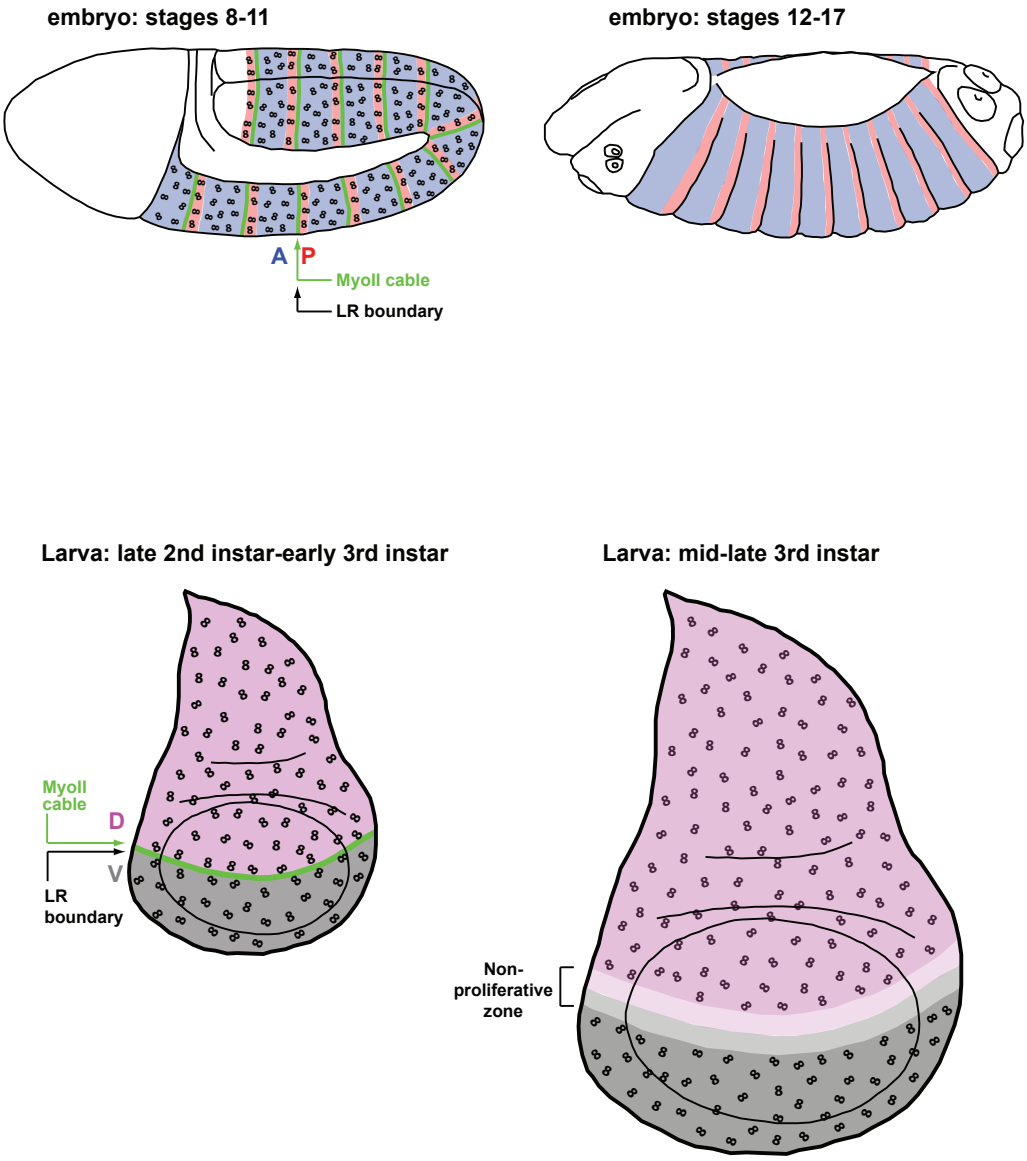

Figure S6 Correlation between MyoII cabling and cell division at compartmental boundaries in *Drosophila*. In the embryo, MyoII cables are observed at parasegmental boundaries at stages 8-11 (Fig. 2a and Fig. S3d), when epidermal cells are mitotically active[6]. From stage 12 onwards, loss of MyoII cable correlates with cessation of epidermal cell divisions. It is also at this stage that parasegmental grooves, an anatomical manifestation of lineage restriction at parasegmental boundaries, disappear[3, 4]. It is likely that these grooves are caused by MyoII-based asymmetric cortical tension (see Fig. S3d, e). We propose that MyoII cables are no longer required to maintain straight boundaries after stage 12 because movements of cells relative to each other, which are caused mainly by cell divisions, but also occasionally by cell intercalation or ingression, have stopped. At stage 12 and after, the morphogenetic processes such as germ-band retraction and dorsal closure rely on cell shape changes rather than cell movements[3, 7]. At the dorsal-ventral (DV) boundary of the *Drosophila* wing disc, a boundary of lineage restriction is present between second (L2) and late third (L3) instar stages[8, 9]. An actomyosin cable transiently forms at the DV boundary during L2-early L3 stages[10, 11], before the establishment of a non-proliferation zone a few cells wide on each side of the DV boundary during mid-late L3 stages[12, 13]. Although a requirement for the Myo II cable has not been tested directly here, we propose based on our data in the embryo, that in the disc as well the function of the MyoII cable would be to correct cell mixing while cell divisions are active at the boundary. This function would cease once the non-proliferation zone is in place. LR boundary: lineage restriction boundary; NPZ: non-proliferation zone.

Supplementary Movies Legends

Movie S1 MyoII cables at parasegmental boundaries are dynamic structures. Time-lapse movie of ectodermal cells in a *MRLC-GFP* embryo during germ band extension. Ventral view, anterior is to the left. Arrowheads at the midline point at the MyoII cables, which are segmentally repeated. During the movie, clusters of divisions occur in the lateral ectoderm and occasionally deform the MyoII cables. Note that at the end of the movie, the embryo rolls on its side and a more ventral-lateral view can be seen. On this view, four MyoII cables (corresponding to parasegments T2-A2) are seen, highlighting the continuity of the structure from the ventral midline to the dorsal edge of the ectoderm.

Movie S2 Divisions of boundary cells transiently deform the MyoII cable. Time-lapse movie showing a parasegmental boundary in a *MRLC-GFP* embryo, with the MyoII cable coloured in green. Anterior is to the left. Dividing boundary cells (stars) deform the MyoII cable (arrows) and transiently invade the opposite compartment. After division, the daughter cells always go back to their compartment of origin and the boundary straightens out.

Movie S3 Cell mixing following inactivation of MyoII at the parasegmental cable by GFP-based CALI. Time-lapse movie showing a parasegmental boundary after CALI in a *MRLC-GFP* embryo. This movie corresponds to the case shown in Fig. 5a. Violet, cyan, red and blue cells are initially in the anterior compartment, while orange, green and yellow cells are in the posterior one. The movie starts just after CALI, which has inactivated MyoII at the cable present at the interface between anterior and posterior compartments. At the beginning of the movie, the red cell, which is rounding up prior to division, has deformed the boundary. In contrast to wild-type, in absence of MyoII at the cable the red daughter cells are not pushed back in the anterior compartment, and the right-hand side daughter cell invades the posterior compartment, leading to compartmental cell mixing.

Supplementary references

1. Chandraratna, D., Lawrence, N., Welchman, D.P. & Sanson, B. An in vivo model of apoptosis: linking cell behaviours and caspase substrates in embryos lacking DIAP1. *Journal of Cell Science* **120**, 2594-2608 (2007).
2. Vincent, J.P. & O'Farrell, P.H. The state of engrailed expression is not clonally transmitted during early Drosophila development. *Cell* **68**, 923-931 (1992).
3. Martinez-Arias, A. Development and Patterning of the Larval Epidermis of Drosophila, in *The development of Drosophila melanogaster*. (ed. M.A.E. Bate) 517-6081993).
4. Larsen, C., Bardet, P.L., Vincent, J.P. & Alexandre, C. Specification and positioning of parasegment grooves in Drosophila. *Dev Biol* **321**, 310-318 (2008).
5. Bertet, C., Sulak, L. & Lecuit, T. Myosin-dependent junction remodelling controls planar cell intercalation and axis elongation. *Nature* **429**, 667-671 (2004).
6. Campos-Ortega, J.A. & Hartenstein, V. The embryonic development of Drosophila melanogaster. *Berlin: Spinger-Verlag* **2nd edn**, 287-308 (1997).
7. Schock, F. & Perrimon, N. Cellular processes associated with germ band retraction in Drosophila. *Dev Biol* **248**, 29-39 (2002).
8. Dahmann, C. & Basler, K. Compartment boundaries: at the edge of development. *Trends Genet* **15**, 320-326 (1999).
9. Irvine, K.D. & Rauskolb, C. Boundaries in development: formation and function. *Annu Rev Cell Dev Biol* **17**, 189-214. (2001).
10. Major, R.J. & Irvine, K.D. Influence of Notch on dorsoventral compartmentalization and actin organization in the Drosophila wing. *Development* **132**, 3823-3833 (2005).
11. Major, R.J. & Irvine, K.D. Localization and requirement for Myosin II at the dorsal-ventral compartment boundary of the Drosophila wing. *Dev Dyn* **235**, 3051-3058 (2006).
12. Johnston, L.A. & Edgar, B.A. Wingless and Notch regulate cell-cycle arrest in the developing Drosophila wing. *Nature* **394**, 82-84 (1998).
13. O'Brochta, D.A. & Bryant, P.J. A zone of non-proliferating cells at a lineage restriction boundary in Drosophila. *Nature* **313**, 138-141 (1985).